1 Dynamical Cross-correlated Physics Project

– Quantum-beam studies on dynamical cross-correlated physics in strongly-correlated-electron systems –

Project Leader: Hajime Sagayama

Due to strong electron–electron interaction, electrons tend to localize in strongly correlated electron systems. Consequently, spin, orbital occupancy, orbital angular momentum, charge, and lattice serve as degrees of freedom and dominate physical phenomena. When more than one of them simultaneously order (multiferroicity), cross-correlation allows the expression of a non-conjugated external field response such as a change in magnetization by applying an electric field and a change in electric polarization by applying a magnetic field, producing sophisticated features in a monolithic device. In practice, the electric field and magnetic field responses of lattice distortion have already been put to practical use as piezoelectric and magnetostrictive devices, respectively. In comparison, it has been considered difficult to use the correlation between magnetism and ferroelectricity for devices because of its weakness.

Since 2003 when large magnetic field response in ferroelectricity in the spin-driven ferroelectric material $TbMnO_3$ was reported by Kimura et al., such magnetoelectric response has been intensively investigated [1]. A number of new materials showing a huge electromagnetic response have been discovered and developed [2]. Studies of electromagnetic phenomena were initially limited to static or quasi-static operation, but have been extended to the dynamic region because of technological advances in spectroscopic measurements. Indeed, dynamical cross-correlation properties such as huge non-reciprocal directional dichroism of light (see Fig. 2) [3], light-induced phase transition, have been discovered in multiferroic materials [4].

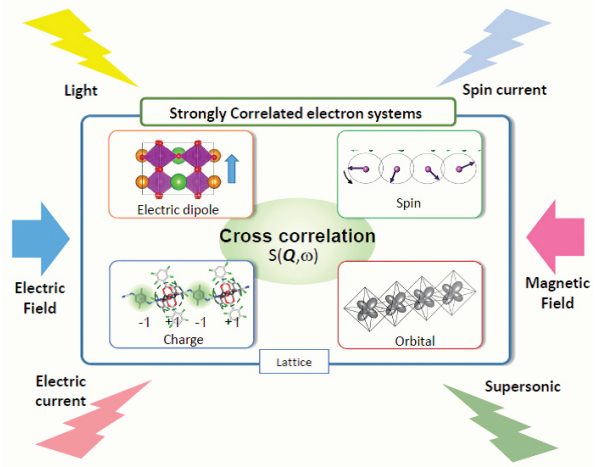

Fig. 1: Schematic view of the cross-correlation among multiple degrees of freedom of spin, electric polarization, charge, orbital, and lattice in strongly correlated electron systems.

The objective of this project is to clarify microscopically the mechanism of the huge cross-correlation properties of strongly correlated and multiferroic materials. The following studies are currently in progress:

1. Direct observation of spin-lattice coupling by circularly polarized X-ray diffraction technique
2. Magneto-ionic phase switching in a metal-organic framework using an Li-ion battery system
3. Microscopic mechanism of large dynamical and static electromagnetic response in $Co_4Nb_2O_9$
4. Electronic polarization induced by orbital ordering in the A-site ordered perovskite manganites

In this text, only the first and second studies are described due to lack of space.

1-1 Direct observation of spin-lattice coupling by circularly polarized X-ray diffraction technique (K. Tokumura, K. Matsuura et al.,

Tokyo Univ.)

Theoretical studies by Katsura and Sergienko independently proposed that spin and electric polarization connect through the inverse effect of the Dzyaloshinskii-Moriya (DM) interaction in multiferroic materials [5,6]. Katsura demonstrated how non-collinear spin arrangement produces local electric polarization with a cluster model in several situations. They qualitatively succeeded in explaining magneto ferroelectricity in cycloidal-type multiferroic materials. However, it is difficult to reproduce the value and direction of polarization even in representative cases such as $TbMnO_3$ and $MnWO_4$. This model is oversimplified for application to real materials in

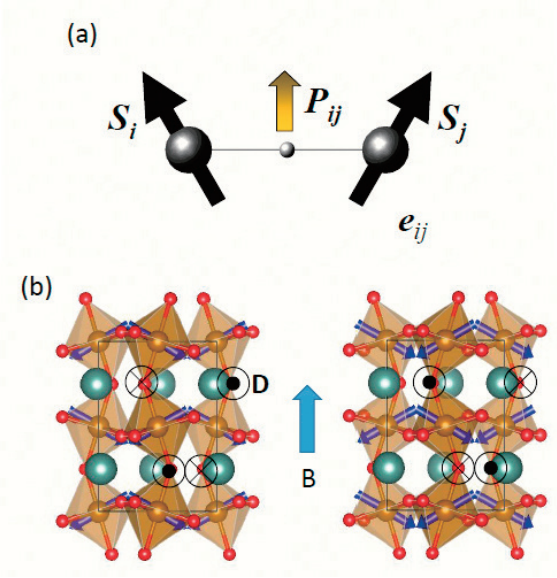

Fig. 2: (a) Schematic view of the inverse DM interaction. (b) Two types of possible phase relation between G-type antiferromagnetic spin arrangement and FeO_6 tilting pattern. The difference between them is due to the sign of the D vector.

which the electric polarization is produced due to uniform shift of the electronic clouds as well as that of ions. Such shift had not been detected by microscopic probes because of its smallness. For the first step, we have tried to detect a coupling between the non-collinear spin arrangement and the local ionic shift through the DM interaction.

The DM interaction is formalized as

$$\mathrm{E_{DM}} = \mathbf{D}(\mathbf{S_i} \times \mathbf{S_j}) \quad (1)$$

where, D is a vector determined by spin orbit coupling and antisymmetric shift of an ion between two adjacent spins, $\mathbf{S}_i$ and $\mathbf{S}_j$ [7,8]. It makes collinear spins tilt and thus produces a weak ferromagnetism in some kinds of anti-ferromagnetic materials possessing zigzag-chain-like lattice modulation. The orthoferrite $YFeO_3$, which crystallizes in a distorted perovskite structure (see Fig. 2), was selected as a target material. Since trivalent Fe ions in this material are surrounded by a divalent oxygen-forming octahedron, the fivefold degenerate 3d-electronic state splits into the threefold degenerate t_{2g} orbital and the twofold degenerate e_g orbital. High-spin state with S = 5/2 is caused by the strong electronic interaction and consequently it possesses no orbital degrees of freedom. The spins align along the *a* axis and form the so-called G-type antiferromagnetic structure at room temperature as shown in Fig. 2. Since FeO_6 octahedrons alternately tilt, D vectors are also alternately aligned. Therefore, the DM interaction works to cant Fe spins and consequently produce the A-type antiferromagnetic structure with tiny b component and F-type ferromagnetic structure with tiny *c* component. There are two possible phase relations between spin direction and FeO_6 tilting as shown in Fig. 2. The difference between them is due to the sign of the D vector.

The X-ray cross section for nonresonant charge and magnetic scattering was formulated by Blume and Gibbs as

$$\begin{aligned}\frac{d\sigma}{d\Omega} &\propto F(\mathbf{K})^2(1+\cos 2\theta^2) \\ &\mu 4\frac{\eta\omega}{mc^2}F(\mathbf{K})^2 S_1(\mathbf{K})\cos\theta\sin^2\theta(1+\cos 2\theta) \\ &+\left(\frac{\eta\omega}{mc^2}\right)^2 S_1^2(\mathbf{K})\cos^2\theta\sin^4\theta(1+\cos 2\theta)^2\end{aligned} \quad (2)$$

where, F(K) and S(K) are charge and magnetic scattering structure factor, respectively [9]. θ is the scattering angle. The first and third terms correspond to the charge and magnetic scattering terms, respectively. The third term is purely magnetic and is negligible in this study because of its smallness. The second term is the cross term of charge and magnetic scattering, which becomes zero in the case of a linearly polarized X-ray beam. If the incident X-ray is circularly polarized, the second term could survive. The sign of the cross term is inverted when the rotation direction is circular polarization. It is also reversed by spin flip.

Circularly polarized X-ray diffraction measurement was carried out at BL-3A, PF. A schematic view of the setup is shown in Fig. 3. The X-ray

beam was monochromatized using a Si(111) double-crystal monochromator, while higher-order harmonics were attenuated using a platinum-coated mirror. A 1.2-mm-thick diamond phase retarder in a transmission geometry of (220) Bragg diffraction was used to convert the polarization from linear to circular. The polarization state of the transmitted beam was controlled by changing the offset angle from the Bragg diffraction conditions. A single-crystal sample of $YFeO_3$ grown by the floating zone method was cut into a rectangular shape. The widest surfaces were

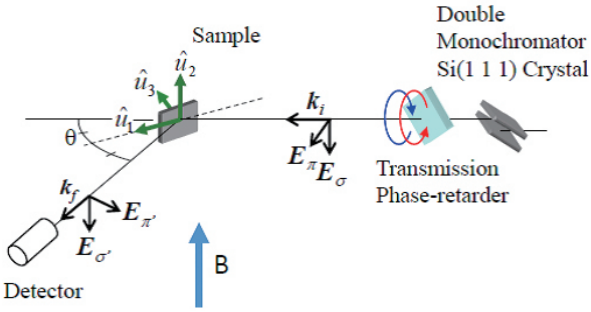

Fig. 3: Schematic view of the experimental setup, including the coordinate system. *k*i and *k*f are the incident and scattered wave vectors. *E*σ (*E*σ') and *E*π(*E*π') are the polarization components of the incident (scattered) X-ray perpendicular and parallel to the scattering plane.

approximately normal to the scattering vector and were polished with alumina powder. The sample was subsequently placed in a closed-cycle He refrigerator mounted on a Huber diffractometer.

The experimental results are shown in Fig. 4. The (1 4 -1) reflection intensity was measured at T ~ 210 K under magnetic fields B = +1T and –1T; it changes depending on the offset angle of the diamond phase retarder. A systematic difference of magnetic field direction can be clearly detected as shown in Fig. 4 (b). When polarization is near-perfect circular, the difference dI = I(B = 1T) – I(B = –1T) becomes large. The sign of dI for left-hand-circular (LHC) polarization and that for right-hand-circular (RHC) polarization are opposite, because the spin direction of the antiferromagnetic component is reversed by switching the direction of the magnetic field. Based on the experimental result, we can estimate the relation between the FeO_6 tilting and the D vector direction. This study is a good example showing the utility of the circularly polarized X-ray diffraction technique for investigating spin and lattice coupling.

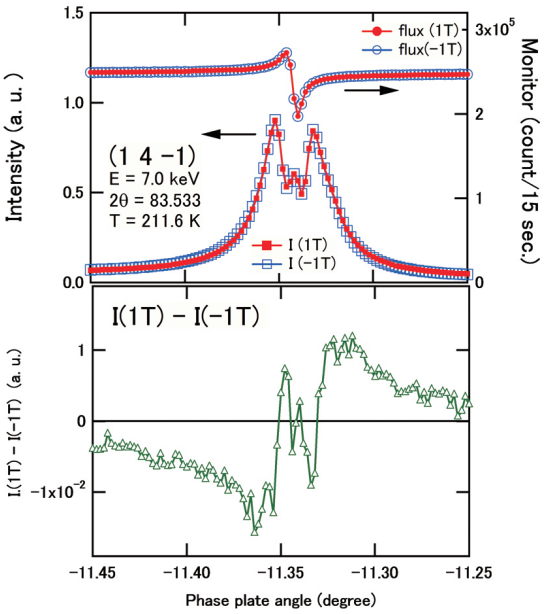

Fig. 4: Offset-angle dependences of the (14-1) reflection for incident X rays at 7.0 keV under magnetic fields +1T and -1T.

1-2 Magneto-ionic phase switching in an electron-donor/-acceptor metal-organic framework using an Li-ion battery system (K. Taniguchi et al., Tohoku Univ.)

Electrical control of magnetism has been of great interest in the fields of materials science and spintronics [10]. In these research fields, various approaches for controlling electrical magnetism, such as magnetic domain reversal by polarized spin-current flow and electric-field modulation of magnetic anisotropy, have been suggested and demonstrated so far. Electron-filling control using a field effect transistor (FET) in correlated electron systems is another main approach for modulating magnetic properties by electrical means. In diluted magnetic semiconductors, the stability of ferromagnetic phase is successfully controlled by tuning electron density using FET systems. However, application of FET systems is inevitably limited to thin films or materials interfaces because of the electrostatic screening effect of electric-field-induced carriers, which prevents penetration of the electric fields into the bulk region.

Recently, Li-ion battery (LIB) systems have been attracting attention as another type of device for filling control, which is applicable for bulk materials [11,12,13]. In an LIB system, Li-ion migration accompanied by a redox reaction in electrodes

is used for energy storage. This mechanism can be used to control the electron density of the electrode materials, because an equal number of electrons and Li^+ ions are introduced to the electrode materials to maintain charge neutrality. In our recent study, taking advantage of this LIB characteristic, we attempted to control electrical magnetism in bulk compounds by the Li-ion migration that accompanies redox reactions, i.e. 'magneto-ionic control' [14].

As a target material, we selected the electron-donor/-acceptor metal-organic framework (D/A-MOF), which is composed of paddlewheel-type diruthenium(II, II) complex as a donor (D) unit, and 7,7,8,8-tetracyano-*p*-quinodimethane (TCNQ) derivative as an acceptor (A) unit. Since the D/A-MOFs are porous redox-active compounds, they are suitable for the electrodes of LIB systems. A notable characteristic of D/A-MOFs is that the magnetic order appears when A is in a radical state with an unpaired spin. Focusing on this characteristic, we have carried out selective electron-filling control of the A-sites in the paramagnetic neutral D/A-MOF, in which A-sites have no radical spins, through tuning of battery voltage in discharge/charge cycles (Fig. 5(a)). In this study, to obtain a neutral system for magnetism control, a combination of $[Ru_2^{II,II}(CF_3CO_2)_4(THF)_2]$ and BTDA-TCNQ, which have a positive $\Delta E_{H\text{-}L}(DA) \equiv E_{LUMO}(A) - E_{HOMO}(D)$ value, was chosen to suppress electron transfer from D to A. Indeed, this D/A combination resulted in the new neutral D_2A-type layered MOF, $[\{Ru_2^{II,II}(CF_3CO_2)_4\}_2(BTDA\text{-}TCNQ)]\cdot n CH_2Cl_2\cdot(p\text{-xylene})$ (**1**) (Fig. 6(a)). In the electron-filling control by an LIB system, since Li-ion insertion into the target material is necessary, we removed the crystal solvent CH_2Cl_2 by evacuating **1** to produce space for accommodating Li-ions. For the CH_2Cl_2 removed compound, $[\{Ru_2^{II,II}(CF_3CO_2)_4\}_2(BTDA\text{-}TCNQ)]\cdot(p\text{-xylene})$ (**1'**) (Fig. 6(b)), we attempted electron-doping through Li-ion insertion. Figure 5(b) displays the temperature dependence of magnetization of pristine (**1'**) and Li-ion inserted samples: $Li_x[\{Ru_2^{II,II}(CF_3CO_2)_4\}_2(BTDA\text{-}TCNQ)]\cdot(p\text{-xylene})$.

A rapid increase of magnetization at around 80 K is observed for the Li-ion-inserted sample at

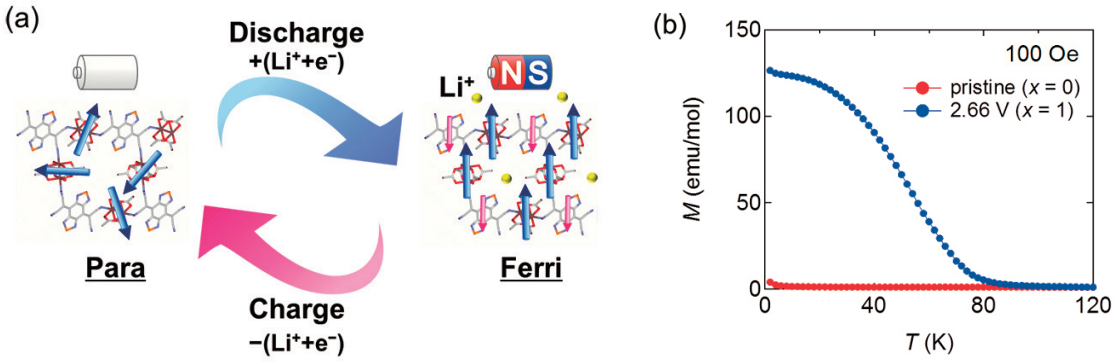

Fig. 5: (a) Schematic figure of magnetism control in D/A-MOF by an LIB system. (b) Magnetic phase switching by Li-ion insertion.

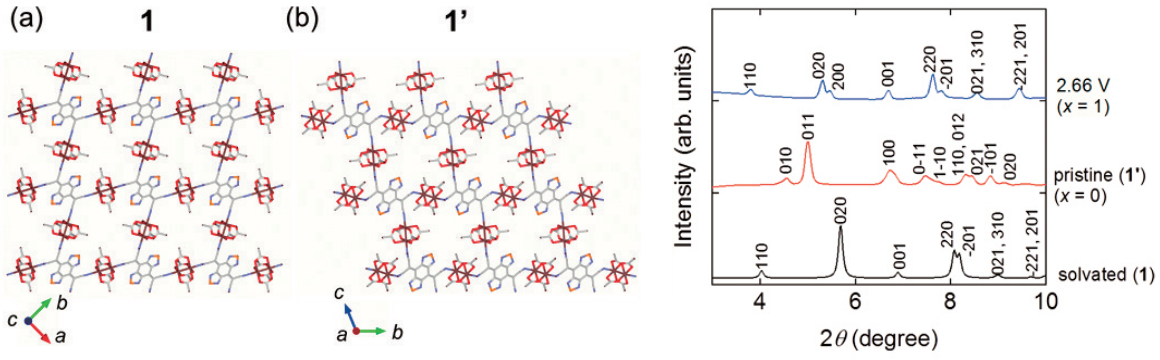

Fig. 6: (a) The crystal structure of as-synthesized sample containing CH_2Cl_2 (**1**). (b) The crystal structure of dried sample (**1'**) after removal of CH_2Cl_2. (c) The PXRD patterns for the pristine (**1'**) (red line) and the Li-ion-inserted material (2.66 V vs. Li/Li^+) (blue line). The pattern of **1** is shown for comparison (black line).

2.66 V vs. Li/Li^+ (x = 1). This result indicates that the ferrimagnetic order is induced from the paramagnetic state by electron-filling of BTDA-TCNQ units through Li-ion insertion (Fig. 5(a)). Furthermore, we succeeded in reversible phase switching with the discharge/charge cycle of an LIB system between the paramagnetic and ferrimagnetic states (Fig. 5(a)).

The structural variation driven by the accommodation of Li-ions in **1'** was confirmed by synchrotron X-ray diffraction measurements. Figure 6(c) displays powder X-ray diffraction (PXRD) patterns of the pristine sample (**1'**) (x = 0) and the Li-ion-inserted sample at 2.66 V vs. Li/Li^+ (x = 1). The PXRD pattern of the Li-ion-inserted sample is different from that of **1'**, which crystallizes in the triclinic space group P–1 (Fig. 6(b)). Notably, the PXRD pattern of the Li-ion inserted sample can be indexed to the monoclinic space group C2/m, which is the same as that of the as-synthesized compound **1** containing CH_2Cl_2 (Fig. 6(a)).

These facts indicate that the crystal structure of **1'** is modified during the process of Li-ion insertion and, ultimately, the material adopts a structure similar to that of the CH_2Cl_2 solvated sample (**1**). Li-ions seem to be inserted into the void spaces located in **1'**, which are produced by removal of CH_2Cl_2 from **1**, accompanied by expansion of the flexible framework, like recovering to the structure of **1**, without significant collapse of coordination bonds in the layered framework.

References

[1] T. Kimura, T. Goto, H. Shintani, K. Ishizaka, T. Arima and Y. Tokura, Nature **426**, 55 (2003).

[2] Yoshinori Tokura, Shinichiro Seki and Naoto Nagaosa, Reports on Progress in Physics **77**, 076501 (2014).

[3] N. Kida, Y. Takahashi, J. S. Lee, R. Shimano, Y. Yamasaki, Y. Kaneko, S. Miyahara, N. Furukawa, T. Arima, and Y. Tokura, Journal of the Optical Society of America B **26**, A35-A51 (2009).

[4] H. Ichikawa, S. Nozawa, T. Sato, A. Tomita, K. Ichiyanagi, M. Chollet, L. Guerin, N. Dean, A. Cavalleri, S. Adachi, T. Arima, H. Sawa, Y. Ogimoto, M. Nakamura, R. Tamaki, K. Miyano and S. Koshihara, Nature Materials **10**, 101 (2011).

[5] H. Katsura, A. V. Balatsky, and N. Nagaosa, Phys. Rev. Lett. **98**, 027203 (2007).

[6] I. A. Sergienko and E. Dagotto, Phys. Rev. B **73**, 094424 (2006).

[7] I. Dzyaloshinskii, Journal of Physics and Chemistry of Solids **4**, 241 (1958)

[8] T. Moriya, Phys. Rev. **120**, 91 (1960).

[9] M. Blume and D. Gibbs, Phys. Rev. B **37**, 1779 (1988).

[10] F. Matsukura, Y. Tokura, H. Ohno, Nat. Nano. **10**, 209 (2015).

[11] T. Yamada, K. Morita, H. Wang, K. Kume, H. Yoshikawa, K. Awaga, Angew. Chem. Int. Ed. **52**, 6238 (2013).

[12] S. Dasgupta, B. Das, M. Knapp, R. A. Brand, H. Ehrenberg, R. Kruk, H. Hahn, Adv. Mater. **26**, 4639 (2014).

[13] D. Chen, X. Wang, J. Chen, Z. Ren, M. Xue, G. Chen, Adv. Mater. **27**, 4224 (2015).

[14] K. Taniguchi, K. Narushima, J. Mahin, W. Kosaka, H. Miyasaka, Angew. Chem. Int. Ed. **55**, 5238 (2016).